Nonhydrodynamic aspects of electron transport near a boundary: The Milne problem

Aleksey V. Vasenkov* and Bernie D. Shizgal†
Department of Chemistry, University of British Columbia, 2036 Main Mall, Vancouver, British Columbia, Canada V6T 1Z1
(Received 25 February 2000; revised manuscript received 25 August 2000; published 18 December 2000)

The nonhydrodynamic behavior of electrons near a boundary is studied with the Milne problem of transport theory. A system of electrons dilutely dispersed in a heat bath of atomic moderators is considered in the positive one-dimensional spatial half-space with an absorbing boundary at the origin which mimics an electrode. A flux of electrons is assumed to originate at an infinite distance from the boundary. The Fokker-Planck equation for the electron distribution function in space and velocity is considered. The density and temperature profiles are determined, and the departure from hydrodynamic behavior near the boundary is studied. Argon and helium are chosen as the moderators, and results with different cross sections are obtained. The Fokker-Planck equation is solved with an expansion in Legendre and Speed polynomials, and compared wherever possible with results obtained with a Monte Carlo simulation. The behavior near the boundary is shown to be strongly influenced by the Ramsauer-Townsend minimum in the electron-Ar momentum transfer cross section.

DOI: 10.1103/PhysRevE.63.016401 PACS number(s): 52.25.Fi, 52.40.Hf, 51.10.+y, 02.60.Lj

I. INTRODUCTION

The present paper is directed toward a better understanding of nonequilibrium behavior in a boundary layer near a wall analogous to a plasma sheath. We consider a simple model of the boundary layer which is based on the Milne problem of kinetic theory [1–3], electron transport [4–7], neutron transport [8–10], and/or radiative transfer [11–13]. Our main objective is to consider the departure from hydrodynamic behavior in the boundary layer, and the need for a kinetic theory description. This work overlaps recent papers by Stefanov, Gospodinov, and Cercignani [14] and by Sazhin and Serikov [15].

In the study of electron transport in discharge devices, an important consideration is the nonequilibrium behavior of electrons near an electrode. In realistic devices, this is the region within a mean free path of a wall or electrode, and is referred to as the sheath [16,17]. A description of the nonequilibrium behavior of electrons in such a situation requires the solution of some transport equation such as the Boltzmann and/or Fokker-Planck equations for all charge carriers, and is coupled to the Poisson equation for the self-consistent electric field. The nonequilibrium effects are expected to be large near the boundary, and consequently a hydrodynamic description of the electrons will fail. There have been numerous discussions of these effects in the literature, and the importance of such a study is now very clear [18,19]. This paper is a preliminary study of a simpler system which will provide the basis for a theoretical study of the sheath layer.

The Milne problem refers to the diffusion of a minor constituent or test particle through a background species considered to be at equilibrium. The background species occupies the half-space $r>0$, whereas a vacuum exists in the half-space $r\leqslant 0$ [1]. A current density of magnitude $\bar{j}$ directed in the negative r direction exists in the medium, and it is assumed that there are no other sinks or sources of particles within the medium, but the plane at $r=0$ is an absorbing boundary. The problem consists of determining the steady spatial and velocity distribution of the minor species within the half-space of interest and at the boundary. The main objective is to determine the departure from hydrodynamic behavior near the boundary. From the point of view of electron transport, the important aspect of the problem is the effect that occurs within several mean free paths of the boundary at $r=0$. Far from the boundary, in the positive r direction, hydrodynamic equations are valid; in the present work we use the diffusion equation

$$\bar{j}=-\bar{D}\frac{d\bar{n}^{\mathrm{as}}(r)}{dr} \tag{1}$$

which relates the flux $\bar{j}$, the diffusion coefficient $\bar{D}$, and the gradient of the asymptotic density profile, $\bar{n}^{\mathrm{as}}$. One finds that the extrapolation of the linear asymptotic dependence of the actual density profile intersects the r axis at $r=-q$, where q is the extrapolation length and is a measure of the departure from hydrodynamic behavior. The calculation of the density and temperature profiles, together with the departure from Eq. (1) and the extrapolation length, are the objectives of the present paper. In previous papers, the Milne problem was considered with a hard sphere cross section for test-particle moderator collisions [1] and also for Coulomb collisions [2]. The application to Coulomb collisions was applied to geophysical problems [20] and to the escape of minor species from an atmosphere [21].

The problem of electron diffusion in a model gas near an absorbing boundary was studied with a Monte Carlo method by Braglia and Lowke [5], and with a direct solution of the Boltzmann equation by Lowke, Parker, and Hall [4], Robson [6], and England and Skullerud [7]. The main purpose of these studies is the construction of a model which would explain the results obtained in a Townsend-Huxley experi-

*Permanent address: Institute of Thermophysics, Novosibirsk, 630090, Russia. vasenkov@theory.chem.ubc.ca
†Email address: shizgal@theory.chem.ubc.ca; URL: http://www.chem.ubc.ca/personnel/faculty/shizgal/

ment. Simple analytical formulas for the electron-atom elastic cross section were used by these previous authors so as to avoid many of the mathematical difficulties involved in the solution of the Boltzmann equation. The present paper employs realistic cross sections, and provides an accurate description of boundary effects on electron transport in realistic systems. We also show the inability of hydrodynamic theory to predict the electron energy distribution in the boundary layer correctly.

Here we present a solution of the Milne problem for electrons in a heat bath of atoms. We choose He and Ar as moderators representative of a gas with and without a Ramsauer-Townsend minimum in the electron-atom momentum transfer cross section. Previous researchers [4–7] employed power-law models for the electron-atom collision frequencies, so the influence of the Ramsauer-Townsend minimum in the elastic cross section on the electron transport could not be studied. Owing to the small electron to atom mass ratio, the collision operator in the Boltzmann equation is well approximated by a Lorentz-Fokker-Planck operator [22]. We consider a solution of this Boltzmann equation, subject to appropriate spatial boundary conditions. The distribution function is expanded in Legendre polynomials for the velocity orientation ($\mu=\cos\theta$), and two different basis sets are compared for the expansion of the distribution function in speed (v). Previous works [1,2] considered Laguerre polynomials, the basis set traditionally chosen in kinetic theory, and which is an expansion in the electron energy. However, it was demonstrated [23–25] that polynomials in the electron speed, referred to as speed polynomials, provide a much faster convergence than Laguerre polynomials. In the present work, the formalism of previous papers [1,2] is modified for the use of the speed polynomials and we demonstrate, for a hard sphere cross section, the improved convergence in the application to the Milne problem.

In Sec. II, we provide a brief discussion of the Milne problem and the method of solution with the modifications due to the use of the speed polynomials. Section III presents the results of the calculations for hard spheres as well as for electron-He and electron-Ar momentum transfer cross sections taken from the literature.

II. SOLUTION OF THE MILNE PROBLEM

A. Direct solution of the Lorentz-Fokker-Planck equation

The formalism presented here follows the previous discussions of the Milne problem [1,2]. It is repeated here briefly for completeness, and to show the changes that arise from the use of speed polynomials in place of the Laguerre polynomials. For steady-state conditions, the Fokker-Planck equation for the velocity distribution function of test electrons $\overline{f}(r,v,\mu)$ is

$$v\mu\frac{\partial\overline{f}(r,v,\mu)}{\partial r}=n_1(r)\overline{J}[\overline{f}(r,v,\mu)], \tag{2}$$

where $\mu=\cos(\theta)$, and θ is the angle between $\mathbf{v}$ and the positive r axis, as shown in the previous work [1]. In Eq. (2), $n_1(r)$ is the number density of the background medium, and the linear Lorentz-Fokker-Planck collision operator for elastic electron-atom collisions is defined by [28]

$$\overline{J}[\overline{f}]=\frac{m}{M}\frac{1}{v^2}\frac{\partial}{\partial v}\left\{\left[\sigma(v)v^4\left(1+\frac{kT_1}{mv}\frac{\partial}{\partial v}\right)\right]\overline{f}(r,v,\mu)\right\}+\frac{\sigma(v)v}{2}\frac{\partial}{\partial\mu}\left\{(1-\mu^2)\frac{\partial}{\partial\mu}[\overline{f}(r,v,\mu)]\right\}, \tag{3}$$

where $\sigma(v)$ is the momentum transfer cross section (it is equal to πd^2 for a hard sphere model), M and m are the mass of molecule and electron, respectively, T_1 is the temperature of background medium, and the distribution function of the moderator $\overline{f}_1^M(\mathbf{v}_1')$ is assumed to be characterized by a Maxwellian distribution function $\overline{f}_1^M=(M/2\pi kT_1)^{3/2}\exp(-Mv_1^2/2kT_1)$. We introduce the scaling cross section $\sigma_{sc}=\pi d_0^2$, to rewrite the Fokker-Planck equation in a dimensionless form. With the transformation to dimensionless spatial variable,

$$x=\sigma_{sc}\int_0^r n_1(r')dr', \tag{4}$$

the Fokker-Planck equation can be written in the form

$$p\mu\frac{\partial f(x,p,\mu)}{\partial x}=J[f(x,p,\mu)], \tag{5}$$

where $J=\overline{J}/(\sigma_{sc}v_0)$, $f=\overline{f}[v_0/n_1(r)\sigma_{sc}]^3$, $p=v/v_0$, and $v_0^2=2kT_1/m$. We seek solutions of this equation subject to the boundary condition that no particles in the negative x region return to the medium, that is,

$$f(0,p,\mu)=0,\quad 0<\mu<1.$$

The general solution is written as the sum of a spatial transient part f^{tr} and an asymptotic part f^{as}, that is,

$$f=f^{tr}+f^{as}. \tag{6}$$

The transient solution dominates near the $x=0$ boundary, and it is anticipated that it decays out in a distance of the order of a few mean free paths. The asymptotic solution dominates at large distances where hydrodynamics is expected to be valid.

It was shown in previous papers that the transient solution is of the form

$$f^{tr}(x,p,\mu)=\sum_{k=1}^{\infty}a_k e^{g_k x}R_k(p,\mu), \tag{7}$$

where g_k and $R_k(p,\mu)$ are the spatial eigenvalues and eigenfunctions, respectively, given by

$$J[R_k]=(p\mu)g_k R_k. \tag{8}$$

The eigenfunctions and eigenvalues are determined with the expansion of R_k in the functions $\psi_{nl}(p,\mu)$

$$R_k(p,\mu)=\frac{\exp(-p^2)}{\pi^{3/2}}\sum_{n=0}^{\infty}\sum_{l=0}^{\infty}b_{nl}^{k}\psi_{nl}(p,\mu). \tag{9}$$

which are products of spherical harmonics and speed polynomials $B_n(x)$, that is,

$$\psi_{nl}(p,\mu)=N_l B_n(p)P_l(\mu), \tag{10}$$

and $N_l=\frac{1}{2}\sqrt{\pi^{1/2}(2l+1)}$. The speed polynomials [23–25] are orthogonal with respect to the weight function $w(p)=p^2\exp(-p^2)$, that is,

$$\int_0^{\infty}p^2e^{-p^2}B_n(p)B_m(p)dp=\delta_{n,m}. \tag{11}$$

They satisfy a three term recurrence relation of the form

$$pB_n(p)=\sqrt{\beta_n}B_{n+1}(p)+\alpha_n B_n(p)+\sqrt{\beta_{n-1}}B_{n-1}(p), \tag{12}$$

where the coefficients α_n and β_n are known [26,27]. The eigenvalue problem is then converted to the finite set of linear equations

$$\sum_{n'=0}^{N}\sum_{l'=0}^{L}(A_{nl,n'l'}-g_kB_{nl,n'l'})b_{n'l'}^{k}=0, \tag{13}$$

where $(N+1)$ and $(L+1)$ are the number of speed and Legendre polynomials, respectively. The quantities $A_{n,n'}^{(l)}$ are the matrix elements of the collision operator in the speed basis set, and are defined by

$$A_{nl,n'l'}=\pi^{-3/2}\int e^{-p^2}\psi_{nl}(p,\mu)J(p)\psi_{n'l'}(p,\mu)d\mathbf{p}, \tag{14}$$

For $l=0$, the operator in μ in Eq. (3) does not contribute, and we find that the matrix elements of the operator in v in Eq. (3) are given by

$$A_{n0,n'l'}=-\frac{m}{2M}\delta_{0,l'}\int_0^{\infty}e^{-p^2}[\sigma(p)/\sigma_{\rm sc}]B_n'(p)B_{n'}'(p)p^3dp, \tag{15}$$

where $B_n'(p)$ is the derivative of $B_n(p)$. The recurrence relation for $B_n'(p)$ can be easily obtained with Eq. (12). For $l\geqslant 1$, the operator in v in Eq. (3) makes a negligible contribution because of the small m/M factor. Consequently, the major contribution is from the operator in μ and,

$$A_{nl,n'l'}=-\delta_{l,l'}\int_0^{\infty}e^{-p^2}[\sigma(p)/\sigma_{\rm sc}]B_n(p)B_{n'}(p)p^3dp. \tag{16}$$

It is useful to add the results for a hard sphere (hs) cross section, and we find that

$$A_{nl,n'l'}^{(\rm hs)}=\delta_{l,l'}\frac{\sigma}{\sigma_{\rm sc}}\begin{cases}\sqrt{\beta_{n'+1}}, & n=n'+1\\ \alpha_{n'}, & n=n'\\ \sqrt{\beta_{n'+1}}, & n=n'-1\\ 0, & \text{otherwise.}\end{cases} \tag{17}$$

The quantities $B_{nl,n'l'}$ are the matrix elements of the drift term on the left hand side of Eq. (2). These are given by

$$B_{nl,n'l'}=\begin{cases}\sqrt{\beta_{n+1}}(l+1)/[(2l+1)(2l+3)]^{1/2}, & n'=n+1,\quad l'=l+1\\ \sqrt{\beta_{n+1}}l/(4l^2-1)^{1/2}, & n'=n+1,\quad l'=l-1\\ \alpha_n(l+1)/[(2l+1)(2l+3)]^{1/2}, & n'=n,\quad l'=l+1\\ \alpha_n l/(4l^2-1)^{1/2}, & n'=n,\quad l'=l-1\\ \sqrt{\beta_n}(l+1)/[(2l+1)(2l+3)]^{1/2}, & n'=n-1,\quad l'=l+1\\ \sqrt{\beta_n}l(4l^2-1)^{1/2}, & n'=n-1,\quad l'=l-1\\ 0 \quad \text{otherwise}\end{cases} \tag{18}$$

Numerical diagonalization of the matrices in Eq. (13) gives approximate eigenvalues and eigenfunctions to order $K=(N+1)(L+1)$. As discussed in Ref. [1] and in Ref. [29], the eigenvalues g_k, which includes the zero eigenvalue, occur in positive and negative pairs so that the sum over k in Eq. (7) includes only nonzero negative g_k so that the transient solution is written as

$$f^{\rm tr}(x,p,\mu)=\sum_{k=1}^{(1/2)K-1}a_ke^{g_kx}R_k(p,\mu). \tag{19}$$

The asymptotic solution is written in the form

$$f^{\mathrm{as}}(x,p,\mu) = -(j/D) f^{M}(p)[q + x - \mu U(p)], \qquad (20)$$

where the dimensionless flux and diffusion coefficient are given by $j = \overline{j}/v_0[n_1(r)\sigma_{\mathrm{sc}}]^3$ and $D = \overline{D}/[v_0/n_1(r)\sigma_{\mathrm{sc}}]$, respectively. The function $U(p)$ satisfies the Chapman-Enskog equation for diffusion [30], that is,

$$J[\mu U(p)] = -p\mu, \qquad (21)$$

and is solved with the expansion

$$\mu U(p) = \sum_{n'=0}^{\infty} d_{n'} \psi_{n'1}(p,\mu). \qquad (22)$$

Consequently, the solution of Eq. (21) is given by

$$\sum_{n'=0}^{\infty} A_{n1,n'1} d_{n'} = -\frac{1}{\sqrt{3}}(\alpha_0 \delta_{n,0} + \sqrt{\beta_1}\,\delta_{n-1,0}), \qquad (23)$$

and the diffusion coefficient is given by

$$D = \frac{1}{\sqrt{3}}(\alpha_0 d_0 + \sqrt{\beta_1} d_1). \qquad (24)$$

The general solution is written as in the previous paper [1], and the Marshak boundary conditions are imposed as discussed there. The use of the speed polynomials in the present paper lead to a different result for the matrix $G_{nl,n'l'}$ defined by Eq. (3.3) of that paper. Here we have that,

$$\mathbf{G}_{nl,n'l'} = \boldsymbol{\delta}_{n,n'} \begin{cases} 1/2, & l = l' \\ 0, & l - l', \quad \text{even}; \quad l \neq l' \\ \dfrac{(-1)^{(l+l'+1)/2} l!\, l'! [(2l+1)(2l'+1)]^{1/2}}{2^{l+l'}(l-l')(l+l'+1)\{(l/2)![(l'-1)/2]!\}^2} & \text{otherwise.} \end{cases}$$

B. Monte Carlo method

An alternative to the direct solution of the Boltzmann equation is to use the Monte Carlo method. This method enables one to numerically simulate an experiment instead of solving the Boltzmann equation. In the Monte Carlo simulation, an ensemble of electrons with either a Maxwellian or δ function speed distribution is incident on the gas medium of finite extent in the r direction. The physical size of the medium is chosen large enough so that the steady state electron distribution is reached in a distance of about five mean electron free paths from the left boundary. For a Maxwellian source, the velocity components in cylindrical coordinates (p_r, p_z) for each injected electron are sampled using the Boltzmann statistical distribution with probabilities W_{p_r} and W_{p_z}, and are determined by the equations

$$dW_{p_r} = e^{-p_r^2} d(p_r^2),$$

$$dW_{p_z} = e^{-p_z^2} d(p_z^2).$$

The probability W_φ for the azimuthal coordinate, φ, is sampled from the uniform distribution $dW_\varphi = d(\varphi/2\pi)$. In the case of a δ function source, the radial and longitudinal velocity coordinates of injected electrons are given by $p_r = 0$ and $p_z = 1$, and φ is sampled from a uniform distribution; that is $dW_\varphi = d(\varphi/2\pi)$.

The Monte Carlo simulation follows the electrons through a series of elastic collisions. The path length between collisions is calculated by $l = -\ln(R)/n_1\sigma(v)$, where R is a random number. The energy exchange between electron and atom is neglected. In other words, it is assumed that the ratio of the atomic mass to the electron mass is equal to infinity. We demonstrate later that this procedure gives results in good agreement with the direct solution of the Boltzmann equation in Sec. II A. The neglect of energy exchange in the Monte Carlo simulation is equivalent to setting m/M in Eq. (3) to zero. The polar and azimuthal angles for an electron after each collision are sampled according to an isotropic angular distribution. The electrons that leave the simulation domain are eliminated from consideration. The above procedure is repeated until the steady state distribution of electrons is obtained. Further details of this technique were described elsewhere [31]. The stochastic Monte Carlo simulation could be the most accurate method for the simulation of electron transport if sufficient computer time is available. In this study, up to 10^9 electrons are used to calculate the spatial electron density and temperature profiles.

By monitoring the position and velocity of each electron, one could determine the spatial and velocity distribution of electrons, $n(x,\mathbf{p})$. The electron density is then calculated as given by

$$n(x) = \frac{\Sigma_i n_i(x,\mathbf{p})}{j_0} \frac{1}{\Delta x}, \qquad (25)$$

TABLE I. Comparison of the convergence of eigenvalues with Laguerre and speed basis functions for $L=1$ and $\gamma=10^5$.

	Laguerre	Speed	Laguerre	Speed	Laguerre	Speed	Laguerre	Speed
N	g_1		g_5		g_{10}		g_{20}	
1	0.008 404	0.008 026						
3	0.007 864	0.007 746						
5	0.007 799		0.019 82	0.024 61				
7	0.007 777		0.017 59	0.017 49				
9	0.007 766		0.017 32	0.017 48				
11	0.007 760		0.017 42		0.024 93	0.033 31		
13	0.007 756		0.017 39		0.024 74	0.025 67		
15	0.007 754		0.017 38		0.024 66	0.024 54		
17	0.007 752		0.017 36		0.024 62	0.024 49		
19	0.007 751		0.017 36		0.024 59			
21	0.007 750		0.017 35		0.024 58		0.035 04	0.071 45
23	0.007 750		0.017 35		0.024 56		0.034 90	0.046 19
25	0.007 749		0.017 34		0.024 55		0.034 84	0.038 68
27	0.007 749		0.017 34		0.024 54		0.034 80	0.035 83
29	0.007 748		0.017 34		0.024 54		0.034 77	0.034 84
31	0.007 748		0.017 33		0.024 53		0.034 75	0.034 65
33	0.007 748		0.017 33		0.024 53		0.034 74	0.034 64
35	0.007 748		0.017 33		0.024 52		0.034 73	
37	0.007 747		0.017 33		0.024 52		0.034 72	
39	0.007 747		0.017 33		0.024 52		0.034 71	

where the initial flux electrons is found in the form; $j_0 = \Sigma_k^N j_k$, with N equal to the product of the number of electrons (injected into the gas medium per step) and the number of steps.

The local electron temperature is determined as

$$T(x)/T_1(x) = \frac{1}{3}\sum_i n_i(x,\mathbf{p})[\mathbf{p}_i(x)-\mathbf{V}(x)]^2 \Big/ \sum_i n_i(x,\mathbf{p}), \tag{26}$$

where

$$\mathbf{V}(x) = \sum_i n_i(x,\mathbf{p})\mathbf{p}_i(x) \Big/ \sum_i n_i(x,\mathbf{p}). \tag{27}$$

The summation in Eqs. (25)–(27) is over all electrons in the spatial interval Δx centered at x.

III. RESULTS AND DISCUSSION

The main objective of this paper was to determine the range of validity of the hydrodynamic behavior for electrons near a boundary. The solution of the Boltzmann equation with the Lorentz-Fokker-Planck collision operator was considered. The traditional method of solution of the Boltzmann equation involves the expansion of the distribution function in Legendre polynomials in the velocity orientation and in Laguerre polynomials in the energy. This was the approach in previous papers [1,2]. In this paper, we introduced the use of speed polynomials [23–25] in the solution of the Milne problem for electrons. We showed, for a hard sphere cross section, the accelerated convergence with speed polynomials in comparison with the slower convergence with Laguerre polynomials. Detailed results of the nonequilibrium behavior were then shown for electrons in Ar and He with realistic momentum transfer cross sections.

Table I shows the convergence of the spatial eigenvalues [Eq. (13)] versus the number of polynomials used for a hard sphere cross section [we set $\sigma(v)=\sigma_{sc}$]. The results are shown for $L=1$, because the operator J defined by Eq. (3) is spherically symmetric. The spatial eigenvalues shown for speed polynomials are converged to the significant figures shown. It is clear that the speed polynomials show a much more rapid convergence than the Laguerre polynomials. The results for Laguerre polynomials are obtained as discussed in Ref. [1], whereas the results with speed polynomials are calculated with the formalism in Sec. II. Tables II and III show a similar comparison for the convergence of the diffusion coefficient and the extrapolation length, respectively. For

TABLE II. Convergence of D [Eq. (24)] with N for $L=1$ and $\gamma=10^5$.

N	Laguerre	Speed
1	0.3600	0.3761
3	0.3711	
5	0.3737	
7	0.3747	
9	0.3752	
11	0.3754	

TABLE III. Convergence of extrapolation length with N and L for $\gamma=10^5$.

$L\backslash N$	1	3	5	7	9	11
			Laguerre			
1	0.642	0.660	0.664	0.665	0.666	0.666
3	0.680	0.698	0.702	0.703	0.704	0.704
5	0.682	0.700	0.705	0.706	0.707	0.707
7	0.682	0.701	0.705	0.707	0.708	0.708
9	0.682	0.701	0.705	0.707	0.708	0.708
11	0.682	0.701	0.706	0.707	0.708	0.709
13	0.682	0.701	0.706	0.707	0.708	0.709
15	0.682	0.701	0.706	0.707	0.708	0.709
			Speed			
1	0.667					
3	0.705					
5	0.708					
7	0.709					
9	0.710					

these quantities, the convergence is greatly accelerated relative to Laguerre polynomials. In Table III, the extrapolation length requires only one speed polynomial, whereas up to 11 are required for Laguerre polynomials. It is also interesting to notice that fewer Legendre polynomials are also required in conjunction with speed polynomials.

In Fig. 1, we show the density profiles [in units of $(n_1\sigma_{sc})^3$ for uniform n_1; see Eq. (4.6) of Ref. [1]] for a hard sphere cross section for increasing mass ratios, γ (curves $a-d$) from the solution of the Boltzmann equation analogous to the results reported earlier [1]. For $\gamma\geqslant 100$ there is no change in the density profile. This conclusion supports the

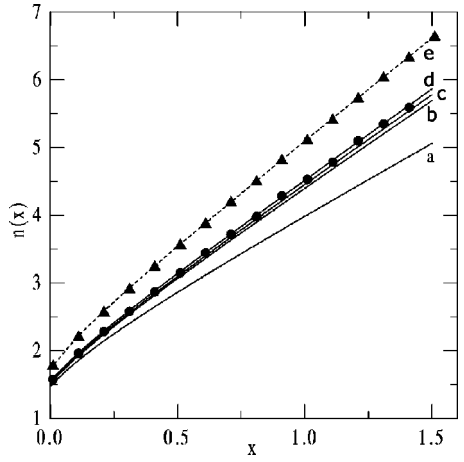

FIG. 1. Density profiles $n(x)$ in units of $(n_1\sigma_{sc})^3$ vs x for hard spheres. Solid lines represent the results of the direct solution of the Boltzmann equation for a Maxwellian source at infinity; the atom to electron mass ratio γ is equal to (curve *a*) 1, (curve *b*) 5, (curve *c*) 10, (curve *d*) $\geqslant$100; circles show a Monte Carlo simulation with a Maxwellian source at infinity (curve *e*). Dashed line, ∞, from LeCaine [32]. Triangles show a Monte Carlo simulation with a δ function source at infinity.

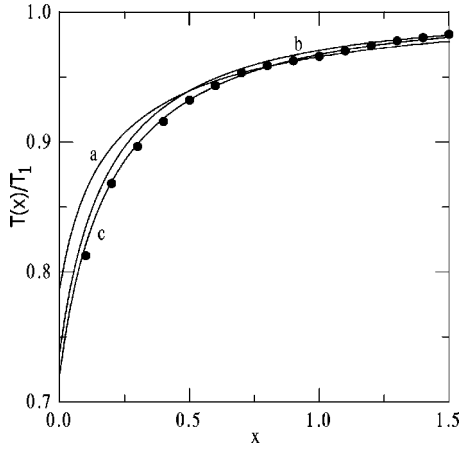

FIG. 2. Temperature profiles $T(x)/T_1$ vs x for hard spheres. Solid lines represent the results of the direct solution of the Boltzmann equation. The atom to electron mass ratio γ is equal to (curve *a*) 1, (curve *b*) 10, and (curve *c*) $\geqslant$100. Circles show the Monte Carlo simulation, with a Maxwellian source at infinity.

correctness of the assumption (used in the Monte Carlo algorithm, Sec. II B) that the energy exchange between electron and gas atom should be neglected for high γ and moderate T_1. In Fig. 1 we present profiles obtained with the Monte Carlo calculation at two different boundary conditions at infinity. The first profile (shown with the circles) was obtained by assuming a Maxwellian source at infinity, which is the same as in the direct solution of the Boltzmann equation in Sec. II A. The agreement with the results obtained with the direct solution of the Boltzmann equation is very good. The second profile (shown with the triangles) is for a δ function source at infinity and is in very good agreement with the results presented by LeCaine [32] (dashed curve). The two profiles for these different choices of distribution function at infinity, Maxwellian (circles) and δ function (triangles), differ owing to the different diffusion coefficients in the two cases. However, as can be seen in Fig. 1, the extrapolation length is independent of this choice of distribution function at infinity. We see that the use of different source functions profoundly influences the results, as mentioned earlier by Williams [33]. This is because there is no energy exchange in atom-electron collisions for γ equal to infinity.

In Fig. 2 we present temperature profiles obtained with the Boltzmann equation for different values of γ. Temperature profiles with Laguerre polynomials were calculated as in previous study [34], while results with speed polynomials were obtained using the expression

$$T(x)/T_1=[2/3n(x)]\Sigma_k a_k e^{g_k x}\{(\beta_1\beta_2)^{1/2}b_{20}^k+\beta_1^{1/2}(\alpha_0+\alpha_1)b_{10}^k+[\beta_1+\alpha_0^2+n(x)^{-2}]b_{00}^k+2/\alpha_0 b_{01}^k+\beta_1^{1/2}b_{11}^k)/(3)^{1/2}n(x)\}+[2/3n(x)D]\times\left\{(q+x)\left[\frac{3}{2}+n(x)^{-2}\right]-2D/n(x)\right\}. \quad (28)$$

Near the wall, the temperature of the electrons, $T(x)$, differs from the temperature of the background gas, T_1. This result

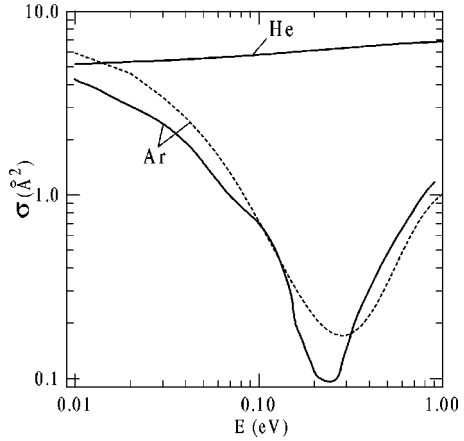

FIG. 3. Momentum transfer cross sections. Data by Mozumder [38] (dashed line) and results from Ref. [37] (solid line); helium data are from Nesbet [36].

is consistent with the measurements obtained by Biondi [35] for diffusion cooling of electrons in gases. Also shown in Fig. 2 are Monte Carlo results, shown as circles, which are in good agreement with the direct solution of the Boltzmann equation.

The application to electron transport in He and Ar is based on the momentum transfer cross sections for these gases shown in Fig. 3. The cross section for He is taken from the calculations by Nosbet [36]. The solid curve in Fig. 3 is the Ar cross section from Ref. [37], whereas the dashed curve is the one from Mozumder [38]. We see that the cross section for He has a weak dependence on energy, while the cross sections in Ar exhibit large Ramsauer-Townsend minima.

The spatial eigenvalues that determine the nature of the transient solution near the boundary, Eq. (7), are shown in Figs. 4(A) and 4(B) for He and Ar, respectively. The value of the scaling cross section, used to obtain the dimensionless form of the Fokker-Planck equation, is chosen equal to 1 Å^2. It is important to note that the ordinate scale for Ar is logarithmic, and that there is a very rapid variation of the eigenvalues with temperature. A very pronounced deep minimum is found for the lower order eigenvalues, and it is shown later how this behavior influences the nonequilibrium behavior near the boundary. By contrast, the variation of the eigenvalues for He is much slower, and essentially linear except at the highest temperatures shown.

The electron density profile near the boundary is shown in Figs. 5(A) and 5(B) for electrons in He. These density profiles are shown as function of dimensionless variable x. This variable was determined with Eq. (4) assuming that $\sigma_{sc} = \pi d_0^2$ with $d_0^2 = 1$ Å$^2/\pi$. We also calculate the density profiles using the hard sphere model. In this case the momentum transfer cross section from Eq. (3) is equal to πd^2, obtained from the requirement that the diffusion coefficient, obtained using a hard sphere cross section, is equal to that obtained with the real cross section. Because the He cross section is weakly dependent on energy, the results with the real cross section (solid line) coincide with those obtained using the effective hard sphere cross section. The density profile ap-

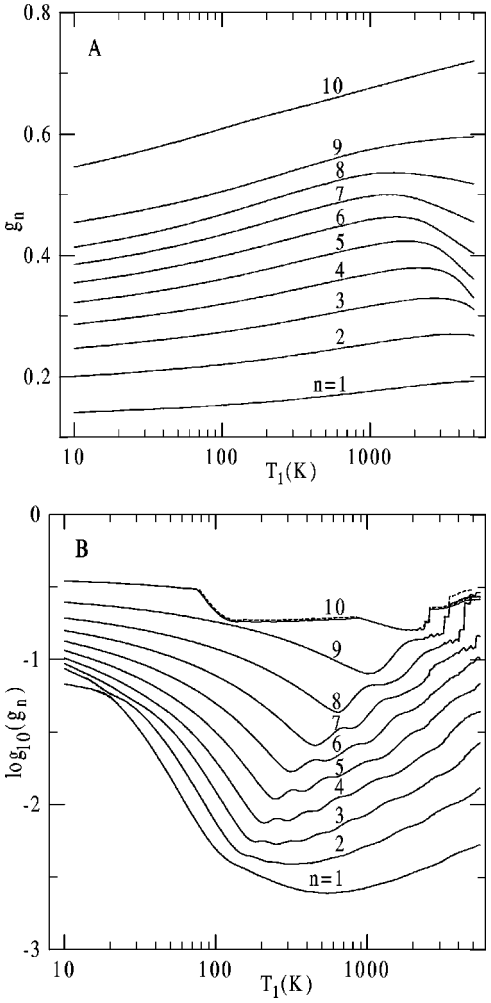

FIG. 4. Temperature variation of the eigenvalues g_n of the Boltzmann collision operator. (A) He, $\gamma = 7297$. (B) Ar, $\gamma = 72818$ solid lines show calculations with $L = 21$ and $N = 11$, while dashed lines represent calculations with $L = 11$ and $N = 11$; $\sigma_{sc} = 1$ Å^2.

proaches asymptotically the linear hydrodynamic profile, $n^{as}(x) = -j(q+x)/D$, obtained using Eq. (20). The extrapolation length q is the intercept on the negative x axis.

Figures 5(C) and 5(D) illustrate the electron density profiles in comparison with the asymptotic profile for electrons in Ar for two different Ar temperatures. As for helium we set σ_{sc} equal to 1 Å^2. With increasing temperature, there are some strong nonequilibrium effects arising from the Ramsauer-Townsend minimum in the electron-Ar momentum transfer cross section. At the lowest temperature, $T = 10$ K, in Fig. 5(C), the density profile exhibits a behavior similar to that obtained for helium. Presumably, only the low energy portion of the momentum transfer cross section is sampled, so that this behavior is characteristic of some effective hard sphere cross section. With an increase in temperature to 300 K [Fig. 5(D)], there is a profound change in the spatial variation of the density profile in that the actual profile (solid curves) does not approach the asymptotic behavior (dashed lines) for the range of x shown. The reason for this behavior is that the spatial eigenvalues [see Fig. 4(B)] decrease rapidly with increasing temperature. The transient so-

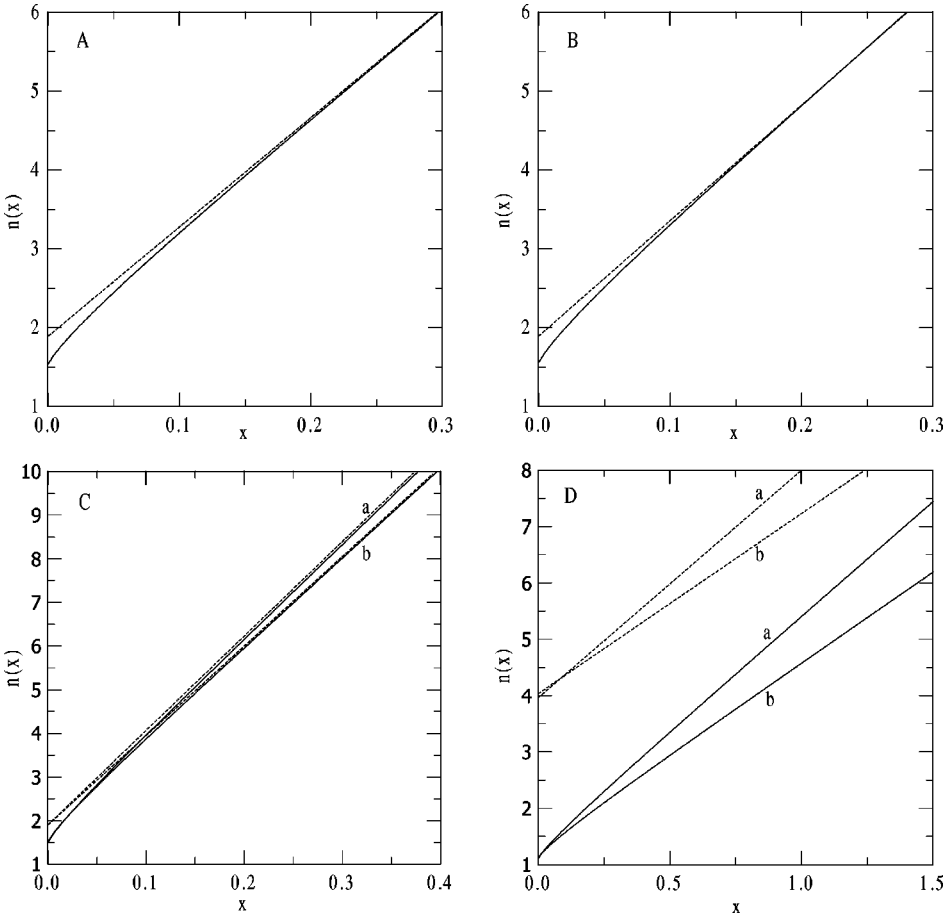

FIG. 5. Electron-density profiles $n(x)$ (solid line) and $n^{as}(x)$ (dashed line) in units of $(n_1\sigma_{sc})^3$ for electrons in helium [(A) and (B)] and argon [(C) and (D)] vs x. The temperature T_1 is equal to [(A) and (C)] 10 K [(B) and (D)] 300 K, $\sigma_{sc}=1$ Å^2. The helium cross section is from Nesbet [36] and the argon cross sections are from (curve *a*) Mozumder [38] and (curve *b*) Ref. [37].

lution decays very slowing with increasing x and persists for many mean free paths; a result that was not anticipated. A comparison of Fig. 5(C) with Fig. 5(D) clearly shows the effect of the Ramsauer-Townsend minimum in the cross section.

Figure 6(A) shows the electron temperature profiles for electrons in He analogous to the results in Fig. 2. The electrons are uniformly cooled below the bath temperature owing to the nonequilibrium effects. The dashed curve, in Fig. 6(A), shows the result using an equivalent hard sphere cross section. By contrast, the results for Ar, shown in Fig. 6(B), exhibit both a cooling and heating, an effect arising from the Ramsauer-Townsend minimum. The four sets of curves labeled $a-c$ in Figs. 6(B) are for increasing moderator temperature. The solid curve is for the cross section reported by Mozumder [38], whereas the dashed curve is the cross section of Ref. [37]. Somewhat analogous cooling and heating effects for model cross sections were discussed by other authors [4]. We see from temperature profiles shown in Figs. 6(A) and 6(B) that the nonequilibrium effects for electrons in Ar persist for larger distances from the boundary than for electrons in He. [This is a manifestation of the minima in the eigenvalues shown in Fig. 4(B).] However, these nonequilibrium effects for the temperature profiles for electrons in Ar are essentially smaller than those found for the density profiles in Figs. 5(C) and 5(D).

A final measure of the nonequilibrium behavior in the boundary layer is the variation of $Ddn(x)/dx$ versus x shown in Figs. 7 and 8 for He and Ar, respectively. Ddn/dx is unity in the hydrodynamic limit. As can be seen in Fig. 7, the nonequilibrium effects in this quantity persist for a fraction of a mean-free-path for electrons in He. Figure 8 shows a similar result for electrons in Ar, where the different curves $a-d$ are for increasing moderator temperature. The solid curve is for the cross section reported by Mozumder [38] whereas the dashed curve is the cross section of Ref. [37]. Although the results persist for larger distances than for He, we do not find the very large nonequilibrium effects, as seen in the density profiles in Fig. 5.

We compare the results obtained using the Boltzmann equation with results of the Monte Carlo simulation for real cross sections in Figs. 9 and 10. The density profiles, calculated with the Boltzmann equation, are compared with the direct simulation results for electrons in Ar and He in Figs. 9(A) and 9(B), respectively. Lines and symbols, labeled by *a* and *b*, represent the results with moderator temperature equal to 100 and 300 K, respectively. The results obtained with the direct solution of the Boltzmann equation are represented by lines, while the Monte Carlo simulation results are shown by symbols. For argon, as moderator, a comparison is presented for two different elastic momentum transfer cross sections. The solid line and filled symbols represent the results with the cross sections from Ref. [38], while the dashed lines and open symbols show the results with the cross sections from Ref. [37]. As shown in Fig. 9, the curves calculated with the Boltzmann equation are in agreement with the Monte Carlo

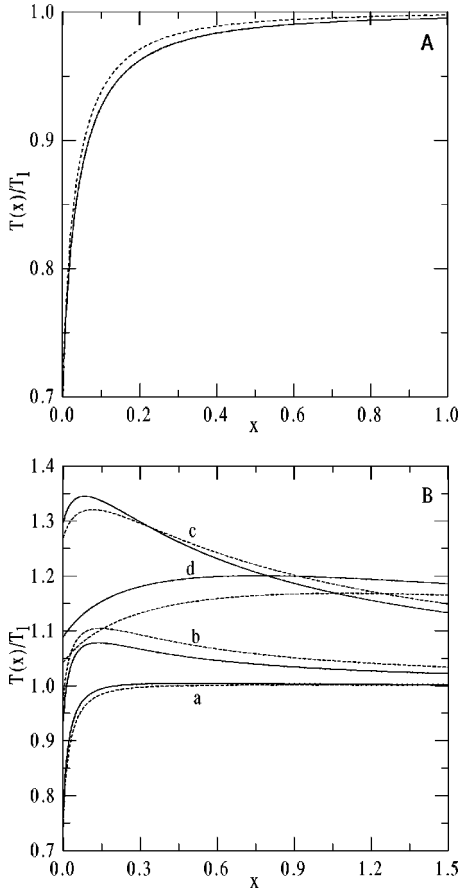

FIG. 6. Temperature profiles $T(x)/T_1$ vs x for electrons. (A) He, $T_1=300$ K; dashed lines show the results with effective hard sphere cross sections, $\sigma=5.505$ Å^2, while solid lines represent results with cross section from Ref. [36] (B) Ar; solid and dashed lines show the results with cross sections from Refs. [38] and [37], respectively; the argon temperature T_1 is equal to (curve *a*) 10 K, (curve *b*) 100 K, (curve *c*) 300 K, and (curve *d*) 1000 K.

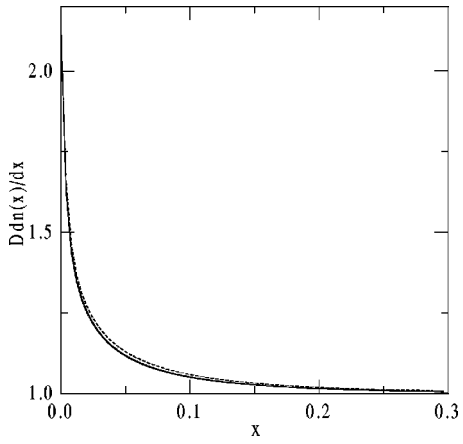

FIG. 7. Ddn/dx for electrons in helium vs x. Cross section from Nesbet [36]. The solid line, shows the effective hard sphere cross section, $\sigma=5.934$ Å^2. The dashed line shows $T_1=1000$ K and $\sigma_{sc}=1$ Å^2.

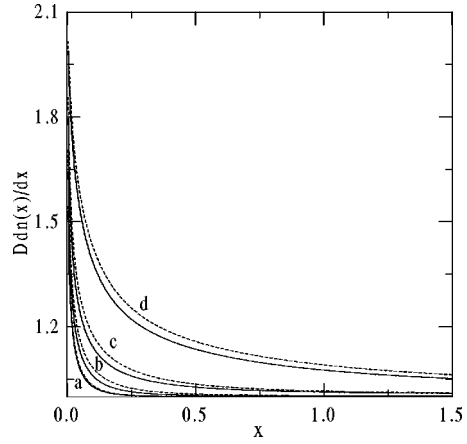

FIG. 8. Ddn/dx for electrons in argon vs x: solid and dashed lines show results with cross section from Refs. [38] and [37], respectively; the argon temperature T_1 is equal to (curve *a*) 10 K, (curve *b*) 100 K, (curve *c*) 300 K, and (curve *d*) 1000 K.

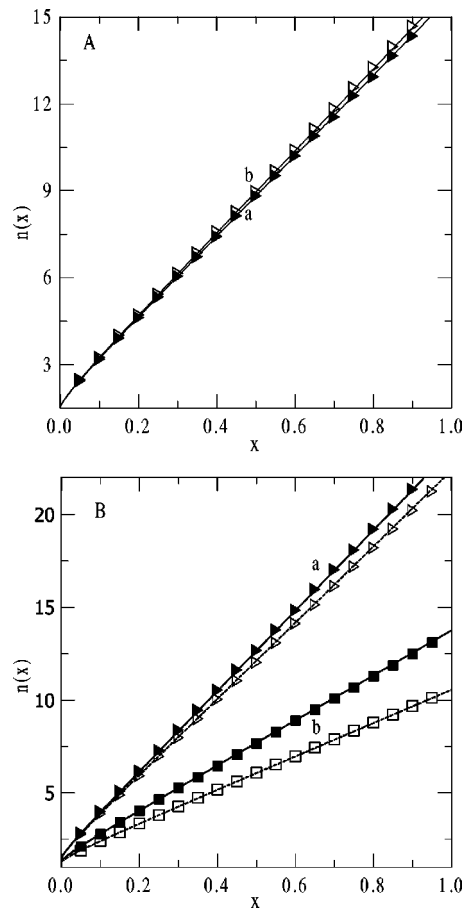

FIG. 9. Density profiles obtained with the Boltzmann equation are compared with Monte Carlo simulation results. Boltzmann equation (solid lines), Monte Carlo simulation (symbols). (A), He; the momentum transfer cross section is from [36]. (B), Ar; solid lines and filled symbols show the results with cross section from Ref. [38], and dashed lines and open symbols represent results with cross section from Ref. [37]. The moderator temperature T_1 is equal to (curve *a*) 10 K and (curve *b*) 100 K.

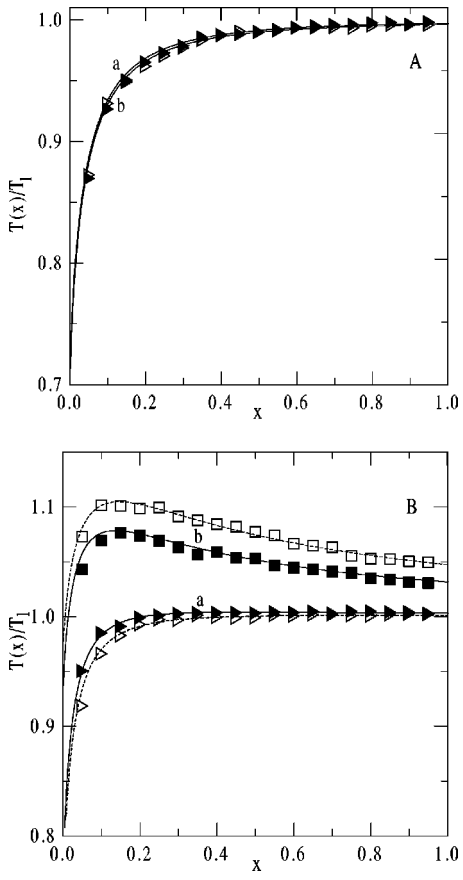

FIG. 10. Temperature profiles obtained with the Boltzmann equation are compared with the Monte Carlo simulation results. Designations and conditions are the same as in Fig. 9.

calculations. A comparison was also made between temperature profiles calculated with the Boltzmann equation and obtained from the Monte Carlo simulation. To show the temperature profiles in Figs. 10(A) and 10(B) we use the same designations as for density profiles. We see in Figs. 10(A) and 10(B) that reasonable agreement is obtained, but is not as good as for the density distributions. This is acceptable as the density is the zero moment of the distribution function, whereas, the temperature is determined by the second moment for which there is a greater number of electrons with energies in the high energy portion of the distribution function.

IV. SUMMARY

A numerical solution of the Boltzmann equation with the linear Lorentz-Fokker-Planck collision operator for the electron transport near the boundary is presented. The method of solution involves the representation of the distribution function by transient and asymptotic portions, and their expansion in basis functions. It was shown for a hard sphere cross section that the convergence of the spatial eigenvalues of the Boltzmann equation with the speed basis functions is considerably faster in comparison to convergence with the Laguerre basis functions. For electrons in Ar, it was also found that the transient part of the solution can be important far from the boundary over several mean free paths. This is attributed to the Ramsauer-Townsend minimum in the momentum transfer cross section. The transient solution decays relatively quickly for electrons in He, for which the momentum transfer cross section has a weak dependence on energy. The results obtained with the direct solution of the Boltzmann equation were compared with a Monte Carlo simulation, and good agreement was obtained. The nonequilibrium effects are large for electrons in Ar owing to the Ramsauer-Townsend minimum in the momentum transfer cross section.

ACKNOWLEDGMENTS

Acknowledgment is made to the Donors of the Petroleum Research Fund, administrated by the American Chemical Society for support of this research (PRF No. 34689-AC6)

[1] M. J. Lindenfeld and B. Shizgal, Phys. Rev. A **27**, 1657 (1983).
[2] J. Barrett, L. Demeio, and B. Shizgal, Phys. Rev. A **45**, (1992).
[3] C. Cercignani, *The Boltzmann Equation and Its Applications* (Springer-Verlag, New York, 1988).
[4] J. J. Lowke, J. H. Parker, and C. A. Hall, Phys. Rev. A **15**, 1237 (1976).
[5] G. L. Braglia and J. J. Lowke, J. Phys. D **12**, 1831 (1979).
[6] R. E. Robson, Aust. J. Phys. **34**, 223 (1981).
[7] J. P. England and H. R. Skullerud, Aust. J. Phys. **50**, 553 (1997).
[8] M. M. R. Williams, *Mathematical Methods in Particle Transport Theory* (Butterworths, London, 1971).
[9] J. J. Duderstadt and W. R. Martin, *Transport Theory* (Wiley, New York, 1979).
[10] K. M. Case and P. F. Zweifel, *Linear Transport Theory* (Addison-Wesley, Reading, MA, 1967).
[11] V. Kourganov, *Basic Methods in Transfer Problems* (Oxford University Press, Oxford, 1963).
[12] K. R. Naqvi, A. El-Shahat, and K. J. Mork, Phys. Rev. A **44**, 994 (1991); K. R. Naqvi, J. Quant. Spectrosc. Radiat. Transf. **50**, 59 (1993).
[13] B. D. Ganapol, J. Phys. A **29**, 1227 (1996); B. D. Ganapol, J. Quant. Spectrosc. Radiat. Transf. **54**, 495 (1995).
[14] S. Stefanov, P. Gospodinov, and C. Cercignani, Phys. Fluids **10**, 289 (1998).
[15] S. S. Sazhin and V. V. Serikov, Planet. Space Sci. **45**, 361 (1997).
[16] J. E. Lawler and U. Kortshagen, J. Phys. D **32**, 3188 (1999); C. Busch and U. Kortshagen, Phys. Rev. E **51**, 280 (1995).
[17] C. A. Ordonnez, Phys. Rev. E **55**, 1858 (1997).
[18] V. A. Godyak and N. Sternberg, IEEE Trans. Plasma Sci. **18**, 159 (1990).
[19] M. Surendra, D. B. Graves, and G. M. Jellum, Phys. Rev. A **41**, 1112 (1990).
[20] O. Lie-Svendsen and M. H. Rees, J. Geophys. Res. **101**, 2415 (1996).

[21] A. R. Barakat and J. Lemaire, Phys. Rev. A **42**, 3291 (1990).
[22] M. Mitchner and C. H. Kruger, *Partially Ionized Gases* (Wiley, New York, 1973).
[23] B. Shizgal, J. Chem. Phys. **70**, 1948 (1979).
[24] B. Shizgal and D. R. A. McMahon, Phys. Rev. A **32**, 3669 (1985).
[25] B. Nowakowski, Physica A **255**, 93 (1998).
[26] B. Shizgal, J. Comput. Phys. **55**, 313 (1984).
[27] W. Gautschi, J. Comput. Appl. Math. **12**, 61 (1985).
[28] A. Gilardini, *Low Energy Electron Collisions in Gases: Swarm and Plasma Methods Applied to Their Study* (Wiley, New York, 1972).
[29] K. Frankoswki, Z. Alterman, and C. L. Pekeris, Phys. Fluids **8**, 245 (1965).
[30] S. Chapman and T. G. Cowling, *The Mathematical Theory of Nonuniform Gases* (Cambridge University Press, Cambridge, England, 1970).
[31] A. V. Vasenkov, Phys. Rev. E **57**, 2212 (1998).
[32] J. LeCaine, Can. J. Res., Sect. A **28**, 242 (1950).
[33] M. M. R. Williams, Nucl. Sci. Eng. **18**, 260 (1964).
[34] Equation (4.8) from Ref. [1] should be written
$$T(x)/T_1=[2/3n(x)]\Sigma_k a_k e^{g_k x}\{-(\tfrac{3}{2})^{1/2}b_{10}^k + [\tfrac{3}{2}+n(x)^{-2}]b_{00}^k+2^{1/2}b_{01}/n(x)\} + [2/3n(x)D]\{(q+x)[\tfrac{3}{2}+n(x)^{-2}]-2D/n(x)\}.$$
[35] M. A. Biondi, Phys. Rev. **93**, 1136 (1954).
[36] R. K. Nesbet, Phys. Rev. A **20**, 58 (1979).
[37] M. Suzuki, T. Tanigushi, and H. Tagashira, J. Phys. D **23**, 842 (1990).
[38] A. Mozumder, J. Chem. Phys. **72**, 1657 (1980).